Multi-year eddy-covariance measurements at a pre-alpine humid grassland site: Dataset overview, drought responses, and effects of land management

Author(s):
Michel, Dominik; Seneviratne, Sonia I.

Publication date:
2022-11-15

Permanent link:
https://doi.org/https://doi.org/10.3929/ethz-b-000572786

Originally published in:
Agricultural and Forest Meteorology 326, https://doi.org/10.1016/j.agrformet.2022.109166

Agricultural and Forest Meteorology 326 (2022) 109166

Contents lists available at ScienceDirect

Agricultural and Forest Meteorology

journal homepage: www.elsevier.com/locate/agrformet

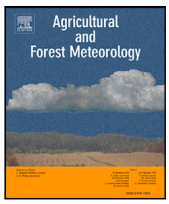

Multi-year eddy-covariance measurements at a pre-alpine humid grassland site: Dataset overview, drought responses, and effects of land management

Dominik Michel *, Sonia I. Seneviratne

ETH Zürich, Department of Environmental Systems Science, Universitätstrasse 16, 8092 Zürich, Switzerland

ARTICLE INFO

Keywords:
Drought monitoring
Gross primary production
Evapotranspiration
Water use efficiency

ABSTRACT

Impacts of drought events on terrestrial ecosystems have been studied extensively in the last decades in light of the long-term human-induced global warming trend and the recent occurrence of severe heat waves and droughts across the globe. The 2003 European summer heat wave sparked high attention towards such events in Switzerland, where ecosystems were largely affected again by summer dry periods in 2015 and 2018. With a newly applied processing scheme of calculating fluxes of net ecosystem exchange of CO_2, latent and sensible heat from eddy-covariance measurements, the impact of droughts on GPP and exchange of energy between land and atmosphere are investigated at a managed grassland site in Switzerland. The rate of primary production is considerably reduced under the influence of dry conditions. This effect is further intensified by grassland management. Evapotranspiration, on the other hand, seems to be unaffected by the lack of precipitation at the site.

1. Introduction

Since the extensive 2003 summer drought-heat event (Fink et al., 2004; García-Herrera et al., 2010; Seneviratne et al., 2012), Europe has again been greatly affected by summer heat waves and droughts in 2015 (Orth et al., 2016; Dong et al., 2017; Hauser et al., 2017; Ionita et al., 2017; Sippel et al., 2017) and 2018 (Hari et al., 2020), with severe impacts on ecological systems (Bastos et al., 2020a; Schuldt et al., 2020; Smith et al., 2020) resulting in extensive consequences for food security and public health across the continent. The recent 6th Assessment report of the Intergovernmental Panel on Climate Change (IPCC AR6) assessed that such events have become more frequent and intense in Central and Western Europe in the observational record, and are projected to further increase in frequency and intensity with increasing global warming (Seneviratne et al., 2021). A comparison of the record-breaking European heat waves in the last two decades with regard to historical records is provided in Hanel et al. (2018), Bastos et al. (2020b), Buras et al. (2020). In Switzerland, the 2015 and 2018 droughts, henceforth named DH1518, had serious consequences such as supply issues in agriculture, low water quality due to warm temperatures, endangerment of water life, and accelerated melting of glaciers (BAFU, 2016; BAFU et al., 2019; Gharun et al., 2020). This study focuses on the response of evapotranspiration (E) and gross primary production (GPP) during dry spells at the managed grassland site Büel-Rietholzbach in a pre-alpine watershed in Switzerland. The used eddy-covariance data series of sensible heat flux (H), latent heat flux (λE) and net ecosystem exchange of CO_2 (NEE) were calculated with a standardized data processing software, in contrast to the processing scheme previously deployed at this site. The new data series are compared in detail to the earlier version of flux calculations. Considerable differences between the two datasets arise mainly from different gap-filling methods. The presented data series will serve as the reference for future use of the data.

The lack of precipitation was most notable in resulting persistently low records of soil water content. Additionally, both the management (grass cutting) and water availability in the two dry years have a large impact on daily GPP, i.e., result in a substantial reduction of primary production in summer compared to average years. The effects of droughts, characterized by low soil moisture levels, on net ecosystem exchange and gross primary production has been documented in several studies, including (Wolf et al., 2014; Zhang et al., 2016; von Buttlar et al., 2018; Stocker et al., 2019; Liu et al., 2020). With a focus on the 2018 European dry spell, the effects have been investigated based on eddy-covariance (EC) measurements by Fu et al. (2020), Ramonet et al. (2020), Thompson et al. (2020), Gharun et al. (2020): In general, these recent studies show that the carbon uptake was lower in 2018 compared to normal years in regions where conditions were dry. Yet, Gharun et al. (2020) found that dry conditions bring high elevations closer to conditions favorable to plant-growth, which led to an increase of GPP of 14% on average at Swiss sites above 1000 m a.s.l. in 2018.

* Corresponding author.
E-mail address: dominik.michel@env.ethz.ch (D. Michel).

https://doi.org/10.1016/j.agrformet.2022.109166
Received 17 December 2021; Received in revised form 7 July 2022; Accepted 11 September 2022

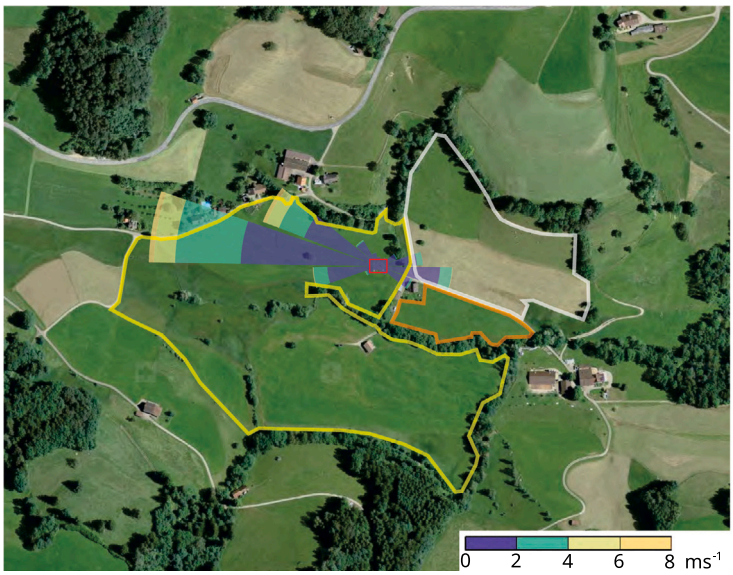

Fig. 1. Observation site Büel-Rietholzbach (rectangle) and surrounding area. The wind rose indicates the frequency (sector size) of wind direction and velocity based on the period 2009 to 2019. For reference, the highest frequency class (daytime westerly wind) corresponds to a frequency of 35%. The outlined areas denote different grassland management schemes. Yellow: cutting, farmer 1; orange: cutting, farmer 2; white: grazing. Aerial view: © 2021 GeoContent, Maxar Technologies. (For interpretation of the references to color in this figure legend, the reader is referred to the web version of this article.)

We investigate here the water, energy and carbon fluxes at a site in northeastern Switzerland, with a focus on the 2015 and 2018 heat and drought events. In particular, we also assess the relation between grass management and the grassland response in terms of fluxes, both in normal and extreme years. The results provide valuable new insights on plant–water–carbon relationships in managed grasslands.

The structure of the article is as follows: The methods and data are introduced in Section 2. Results are presented in Section 3. The conclusions are provided in Section 4. We also include an appendix describing the application of a new processing scheme for the eddy-covariance measurements at the site.

2. Material and methods

2.1. Rietholzbach research site

The present study has been conducted at the hydrometeorological research site Büel in the Rietholzbach catchment in northeastern Switzerland (47.38°N, 8.99°E). The pre-alpine hilly catchment drains the relatively small area of 3.31 km^2 and is situated in the Thur river basin, a tributary to the Rhine (Seneviratne et al., 2012). The region is characterized by a temperate humid climate with a mean air temperature (T) of 7.1 °C and abundant precipitation (P) with a mean sum of 1434 mm a^{-1} (data basis 1976–2020). The predominant land cover in the watershed is grassland and pasture (approximately 72%), the vegetation along the creek and on the slopes is dominated by forest (26%), the remaining sparse area is used for settlements. The soil type and depth exhibit a high spatial variability. Overall, shallow Regosols dominate on steep slopes, deeper Cambisols are found in flatter areas, and gley soils are located in the vicinity of small creeks. Since the beginning of the measurements in 1976 land use in the watershed has not changed significantly.

The surrounding vicinity of the observation site is characterized by temporally and spatially moderate management, i.e., cutting of the grass during the growing season (April–October) and grazing by cattle. The effect of vegetation management around the site is most eminent in the signal of net ecosystem exchange, which was measured at this location with an eddy-covariance system. Due to a pronounced mountain–plain circulation the prevailing source area of NEE during the day (westerly wind) is the upvalley grassland slope west of the site. During the night (easterly wind) the prevailing source area is a mix of grassland adjacent to the measurement site and a pasture crop farther in the east, see Fig. 1. For a more detailed description of the Rietholzbach catchment including maps of topography and land use, see Seneviratne et al. (2012). For more information on the research site Büel-Rietholzbach including instrumentation and the surrounding area, see Hirschi et al. (2017), Ruth et al. (2018). Apart from the climatology, which is based on the long-term 1976–2020 measurements, the period analyzed in this study spans from 15 May 2009 until 31 December 2020, covering the time series since the EC measurements have been in operation. For analyses with respect to the annual cycle of EC observations, only full years (2010–2020) are considered.

2.2. Site management

The largest part of the measured NEE footprint area (daytime and nighttime) is a moderately managed grass crop used for producing hay, see Fig. 1. Four to five times a year the grass is cut with a mowing machine at the beginning of the grass heading stage and during dry weather periods. The cutting is performed by two farmers cultivating the land. Typically, the plants are cut down to approximately 5 cm above ground, i.e. the large majority of the biomass is removed within one day. The management periods are shown in Fig. 2. The first and second cutting event usually take place around the end of May and beginning of July, respectively, with approximately one month of growth in between. In 2017, the first cutting was performed considerably earlier, given an almost two months earlier start of the growing season. In late summer and early fall the cutting dates vary largely between years, depending firstly on the plant growth during summer and secondly on the occurrence of dry weather conditions. Generally, there were four cutting events within one growing season except for 2015 and 2017, with five cutting events. Except for the years 2013 and 2015, the last cutting was performed before the end of October. The described cutting regime is mostly affecting daytime NEE, as shown in Fig. 1. The nighttime NEE is additionally influenced by grazed pasture crop east of the observation site. In general, the state of the vegetation in the nighttime footprint is comparable to that of the daytime conditions.

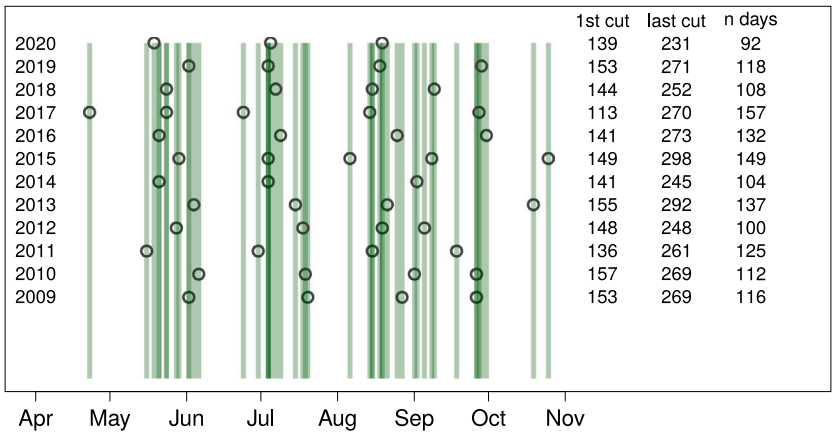

Fig. 2. Overview of cutting dates provided by the farmer for the grassland area around the measurement site Büel-Rietholzbach in single years (circles) and emerging seasonal pattern (vertical lines) from 2009 to 2020. The first cut and last cut of the season are given as day of year, n days denotes the length of the growing season (between first and last cut). The cutting dates 24 Aug 2016 and 24 May 2017 have been determined from visual inspection of GPP data, which indicate cutting events, even though they were not reported by the farmer.

2.3. Flux measurement and data processing

The net ecosystem exchange and fluxes of sensible heat and latent heat (λE_{EC}) presented here were measured using the eddy-covariance method. The subscript in E_{EC} refers to eddy-covariance measurements, as opposed to other mentions of E. The method measures the turbulent vertical exchange of CO_2, sensible heat, and water vapor in a given time interval based on the fluctuations of the desired scalar and vertical wind velocity. The different fluxes are calculated as:

$$NEE = \overline{w'c'} \tag{1}$$

$$H = \rho c_p \overline{w'T'} \tag{2}$$

$$\lambda E_{EC} = \lambda \overline{w'q'}, \tag{3}$$

where w is the vertical wind velocity, c is CO_2 concentration [μmol m^{-3}], T is temperature [K] and q is the water vapor density [kg m^{-3}]. The prime denotes the turbulent part of the measured variable. ρ is the density of air, c_p is the specific heat capacity of air and λ is the heat of vaporization. The fluxes were measured using an eddy-covariance system consisting of a CSAT3 ultrasonic anemometer (Campbell Scientific Inc., USA) and an infrared open-path gas analyzer (Li-7500, LI-COR Biosciences, USA), mounted on a tower at 2 m above ground in the southeast corner of the observation site Büel-Rietholzbach. The horizontal separation distance between the gas analyzer and the sonic anemometer was 0.2 m. A sampling rate of 10 Hz was used. The instrumental set-up of the EC measurements has been described comprehensively in Hirschi et al. (2017), hereafter referred to as H17. Apart from filtering data when turbulence was disturbed by the EC tower, i.e., in cases of wind directions between > 310 and < 50 degrees (see H17) the raw data processing, data filtering as well as the gap-filling scheme applied in the present study is different from the H17 data processing scheme. The differences in data processing result in deviations of the calculated fluxes of H17 and the present flux data set, hereafter named M22. The differences are presented in detail in Appendix C.

2.3.1. Flux calculation and filtering

A standard EC data processing tool (EddyPro, LI-COR Biosciences, USA, version 7.0) was newly used for processing raw EC data and calculating fluxes (see also Appendix A). Raw data processing includes spectral correction (Massman, 2000, 2001; Moncrieff et al., 2005) of low-pass and high-pass filter effects, tilt correction (Wilczak et al., 2001), SND-correction (Schotanus et al., 1983) and compensation for air density fluctuations (WPL terms, Webb et al. (1980)) as well as sensor separation in the case of λE_{EC} and NEE. Covariance maximization is applied for detection of time lag between the turbulent components of these two flux variables. The time interval used for averaging high frequency raw data in the present study is 30 min, resulting in a half hourly resolution of the fluxes.

Table 1
Percentage of discarded data after nighttime u_*-filtering based on median bootstrapping ($u_{0.5}$) and after applying all filtering procedures during the night, during the day and in total.

	u_*	*All filters*		
		Night	*Day*	*Total*
NEE	3.40	41.14	15.16	56.3
H	3.40	25.94	13.88	39.8
λE	3.40	29.79	14.65	44.4

The following filtering scheme describes, which data are discarded, i.e., flagged as missing, and are later gap-filled: In the case of precipitation, all EC-derived fluxes were discarded, because liquid water or snow is distorting the sensor signals of the EC system, most importantly those of the gas analyzer. Negative nighttime NEE data (potential shortwave radiation < 10 Wm^{-2}) were discarded, as there cannot be any photosynthesis in the absence of shortwave radiation. In order to avoid a weight shift towards positive nighttime fluxes as a result of this step, a trimmed mean approach was applied on the positive fluxes, i.e., respiration, discarding the same amount of positive as negative values. The data were filtered with the tests for stationarity and well-developed turbulence proposed by Foken and Wichura (1996), Mauder and Foken (2004), rejecting fluxes with the flag 2 for bad turbulence conditions. An additional filtering step for removing cases of low nighttime turbulence intensity was applied using a method based on the relation of NEE and the friction velocity (u_*) within temperature subsets (Papale et al., 2006), see Appendix A. The percentage of missing data after performing the entire filtering procedure is indicated in Table 1 for the individual flux time series. Note that the amount of 3.40 percent of data being discarded due to nighttime u_* filtering represents the case after all preceding filtering steps. In general, more nighttime values are filtered out due to wind direction filtering, which is effective mostly during nighttime conditions, see H17. NEE suffers the largest loss of data due to the nighttime photosynthesis filtering.

NEE is converted from μmol $m^{-2}s^{-1}$ to g C m^{-2} d^{-1} for daily values to be consistent with the units of GPP and ecosystem respiration (Section 2.4).

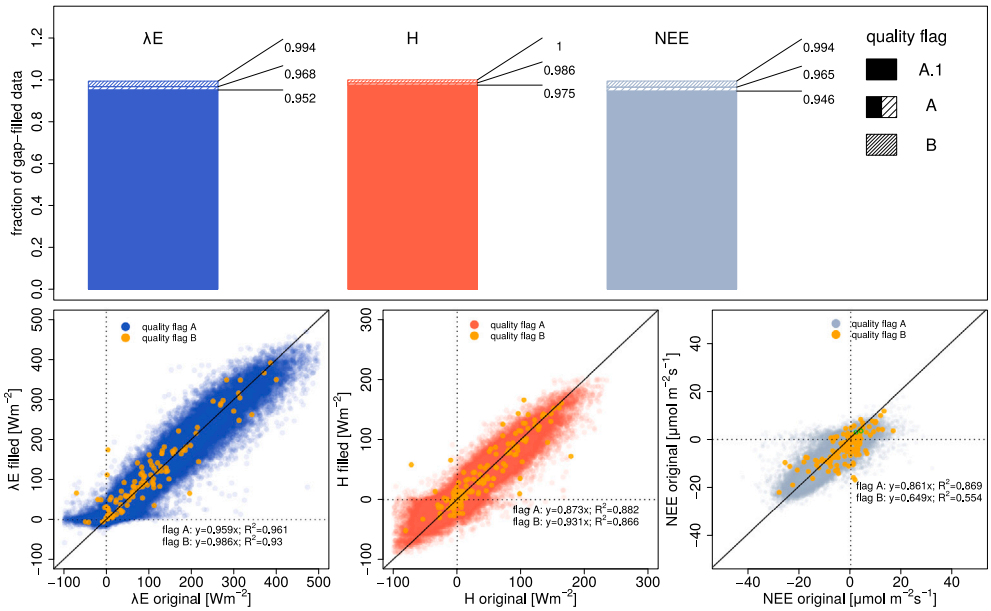

Fig. 3. *Top panel*: Percentage of missing half-hourly values replaced with quality A.1 data (≤ ±7 day window), A data (≤ ±14 days window) and B data (≤ ±28 days window) in the three time series. *Bottom panels*: Correlation of original measurements to estimated half-hourly latent heat flux (*left*), sensible heat flux (*middle*) and CO_2 flux (*right*) data. For quality flag C, no original measurements are available for testing the procedure (<1%).

2.3.2. Gap-filling

After the filtering procedure, gap-filling the half-hourly flux data was performed using the so-called marginal distribution sampling (MDS) by Reichstein et al. (2005a), which relies both on the covariance of fluxes with meteorological conditions (i.e., look-up table approach, LUT) and auto-correlation of fluxes (i.e., mean diurnal cycle approach, MDC).

The LUT approach uses binning of the measured fluxes according to meteorological conditions similar to the missing period, i.e., global radiation (R_{sd}), vapor pressure deficit (VPD) and T. The binned fluxes are averaged to replace the missing values. Similar meteorological conditions are assumed be given, when R_{sd}, T and VPD do not deviate more than 50 Wm^{-2}, 2.5 K and 5 hPa, respectively, within a window of ±7 days of the missing data point. If no according conditions can be found, the window is increased to ±14 days. With still no match, R_{sd} and T are omitted within ±7 days. After still not finding similar conditions with VPD only, the MDC approach is looking for available measured flux data within one hour and then one day, respectively. This procedure is repeated while increasing the window size, if necessary (but not for longer than 60 days). The MDS approach is described in detail in Reichstein et al. (2005a). An accuracy test of the gap-filling procedure yields R^2 correlation coefficients of 0.96, 0.88 and 0.87 for λE, H and NEE between original (measured) and gap-filled data. These correlations represent the case, where the maximum window size of the MDS procedure is 14 days. This accounts for more than 96% of the data (Fig. 3). A more detailed description of the gap-filling performance with the presented data is given in Appendix B.

2.4. Flux partitioning

Partitioning of NEE measurements into daytime GPP and ecosystem respiration (R_{eco}) was performed using the standardized method by Reichstein et al. (2005b,c). Based on nighttime data, when R_{eco} equals NEE, as there is no photosynthetic activity, the temperature sensitivity of R_{eco} is determined with the (Lloyd and Taylor, 1994) model. Using the temperature–respiration relationship, daytime R_{eco} can be used to calculate $GPP = R_{eco} - NEE$.

In order to disentangle cutting effects and meteorological effects on GPP, we established an estimate of its undistorted seasonal cycle at Büel-Rietholzbach using in-situ measurements. Based on the results presented in Fig. 8, data affected by cutting were removed within a window starting 10 days prior to and 21 days after the cutting event. This period is identified as substantially affected by cutting. The resulting gaps were then linearly interpolated between the last and first available data point within the artificial gap. A 15-days running mean filter was applied to this "no-cut" time series to obtain an estimate of the primary production without the cutting effect (GPP_{nc}). An idealized daily time series of the annual GPP seasonality was produced by using the 95th percentile of the 11 daily values of GPP available from 2010–2020 for each day of year in the "no-cut" time series, referred to as GPP_{95}). This step reduces the daily variability of GPP due to meteorological effects. A running mean filter with a window size of 15 days was applied to this time series to smooth out the variability resulting from the rather small sample size per day.

The u_*-filtering, MDS gap-filling and flux partitioning are implemented in the R package ReddyProc (Wutzler et al., 2018).

2.5. Additional measurements

Ancillary data used in the present study for filtering and gap-filling EC data were all measured at the observation site Büel-Rietholzbach next to the EC tower and with a one-hourly resolution. As M22 EC data are half-hourly, the corresponding ancillary hourly value was used for both values of M22 in the respective hour. R_{sd} and the reflected shortwave radiation was measured with CM21 pyranometers, the longwave radiation components were measured with two CG4 pyrgeometers (Kipp & Zonen, Netherlands, ventilated), to calculate net radiation (R_n). T and relative humidity (RH) were recorded with a Thygan VTP6 (Meteolabor, Switzerland). Precipitation was measured with a Joss-Tognini type tipping-bucket gauge mounted at 1.5 m above ground (Lambrecht, Germany). Wind-induced precipitation under-catch was corrected according to Gurtz et al. (2003). Wind velocity and direction was recorded with a propeller wind vane at 10 m above ground (Young, USA). Air pressure was monitored with a PTB100 A barometer (Vaisala, Finland), the storage-corrected ground heat flux (G) was measured as the average of four HFP01 ground heat flux plates at 5 cm depth (Hukseflux, The Netherlands). Air pressure, R_n and G are used to calculate evapotranspiration with the Priestley–Taylor equation, (Eq. (4)).

$$E_{PT} = \alpha \frac{s}{s+\gamma}(R_n - G), \tag{4}$$

where α is the Priestley–Taylor coefficient, s is the slope of the saturation vapor density curve, and γ is the psychrometric constant, see Section 3.

All mentioned sensors have been operational before 2006. Since 1976 and until 2006, long-term data series of T, RH and P have been homogenized as described in Gurtz et al. (2006) and Moesch (2001). The soil water content (θ) was monitored at a depth of 0.05, 0.15, 0.25, 0.35 and 0.55 m with CS616 volumetric water content reflectometers (WCR, Campbell Scientific Inc., USA) since 2009 as part of the SwissSMEX soil moisture network (Mittelbach and Seneviratne, 2012). The chosen depths should reflect the dynamics in water storage in the grass-root zone. The data presented here are integrated soil water content series from depths 0 m to 0.55 m to produce the equivalent soil water column in mm. There are large data gaps of WCR-measured θ from September 2014 to end of July in 2015 when the soil moisture station was not operational due to technical difficulties.

In addition to the long-term data set, a large weighable lysimeter provides hourly evapotranspiration since 1976 (E_{Lys}). Its grass covered surface area is 3.14 m^2 (diameter of 2 m) and the depth is 2.5 m. Gravitational discharge at the bottom is recorded with a 50 mL tipping-bucket. The lysimeter is described in detail in H17 and Ruth et al. (2018). With its measurements the annual change in water storage (ΔS) in mm can be calculated using the water balance equation $\Delta S = P - E_{Lys} - Q_{Lys}$, where Q_{Lys} is the gravitational discharge in mm. The lysimeter-based change in water storage helps describe the inter-annual variability of soil water content, when those measurements are not available in the period 1976–2009. In total for the respective year, a positive value of ΔS indicates that the soil water storage is replenished via precipitation, a negative value indicates that the soil water storage is consumed by evapotranspiration and discharge. ΔS is scaled to mm soil water column equivalent for a soil depth of 0.55 m (instead of 2.5 m) for better comparability with the annual WCR water content. Since 2006, continuous hourly recordings of the total weight of the lysimeter vessel (w_{Lys}) in kg are available. Thus, the annual change in soil water storage could additionally be determined from the annual anomalies of w_{Lys} wrt. to the overall mean, making this record of change in water storage independent of precipitation and discharge measurements, while accounting for the state of the soil moisture in the previous year. The values are scaled to mm soil water column to a depth of 0.55 m. From the w_{Lys} data, a lysimeter-based estimate of daily soil water content (θ_{Lys}) was produced by adding the daily change of water storage to the average of WCR-based soil water content from 2010 to 2020 and scaling with the ratio between the standard deviations of lysimeter-based WCR-based data series. For 2015, the standard deviation of θ in 2018 was used, as not enough data were available. Annual anomalies are calculated as the deviation of annual means from the overall mean of the respective time period, i.e., including DH1518, if not indicated otherwise.

3. Results

The severity of the European summer heat and drought events in DH1518 as observed at the Büel-Rietholzbach research site is clearly visible with regard to the long-term records, as shown in Fig. 4. The discussed dry years stand out as the driest years since 2003 in terms of the precipitation and soil water content as well as ΔS. In the records of air temperature, a general warming trend over the last 45 years is noticeable (0.08 °C per year, p-value 3.2e^{-11}), while the recent records (2015 to 2020) of soil moisture indicate an increase in frequency of dry years compared to the preceding 11-year period since the drought in 2003 (2004–2014). Annual evapotranspiration does not reflect the lack of available water in the dry years, but rather above-average sums, which relates to high photosynthetic activity and soil evaporation due to ample available energy and, most importantly, sufficient water availability even during dry periods. The resilience of soil water availability at the site Büel-Rietholzbach even during pronounced dry spells is underlined by Rassl et al. (2022). Hence, we see rather an increase in annual evapotranspiration from 2010 to 2020 in the case of the EC measurements (11.54 mm per year, p-value 0.02) as function of the available energy indicated by T. In the case of DH1518 and with respect to the long-term time series, T and E_{Lys} lie above the inter-quartile range, P and ΔS lie below the inter-quartile range, which underlines the impact of DH1518 conditions on the environment. Note that the range of E_{EC} in the 11-year time series is substantially higher that the range of the long-term time series of E_{Lys}. This highlights the increasing trend of E mentioned above one the one hand, and is a result of the inherently different methodologies used. A detailed comparison of E observations between lysimeter and EC measurements at the site Büel-Rietholzbach is given in Hirschi et al. (2017). The impact of DH1518 on the hydrological conditions on a seasonal scale at the site Büel-Rietholzbach with regard to the climatological situation is analyzed on the basis of soil water content and precipitation, as well as the turbulent fluxes of heat and CO_2. Apart from precipitation, the seasonal cycle of θ at the Büel-Rietholzbach site is controlled by atmospheric conditions with high soil evaporation and transpiration in summer. The use of soil water for E results in a minimum of soil water storage during June until late August, even when the average amount of daily precipitation is highest (Fig. 5). The annual evolution of θ is characterized by wet periods in winter, when there can also be snow, i.e., January–February and November–December. In between, a drying phase starts mid-March, which is paused from April to beginning of May and then is followed by further drying to a minimum soil water content in July/August. The ample amount of precipitation in summer is thus mostly evaporated rather than put into soil storage. Evapotranspiration is driven by available energy and does not seem to be constrained by water availability. This is reflected in the seasonal cycle of the latent heat flux, which reaches its maximum in summer, when the soil water content is at its lowest level. From August until the end of the year the soil water storage is replenished with P, when E starts to decrease. The consumption of soil water in spring coincides with a drop to negative NEE mid-March, indicating a strong carbon assimilation in the beginning of the growing season, while the average rate of NEE is decreasing towards the end of the growing season. The undulating pattern of NEE as the year progresses is a result from the cutting, with less negative NEE (i.e., reduced sink) after a cutting event, indicating that carbon assimilation is reduced.

The response of soil water content to the precipitation deficit during the dry spells in DH1518 is very distinct. Both dry years stick out with below-average precipitation and soil water content even below the 5th percentile in July/August. In 2015, the soil water content, indicated by θ_{Lys}, was characterized by a surplus due to above-average precipitation amounts in spring (March to mid-May). Both years end with a soil water deficit compared to the long-term average. H and λE are mostly higher than the median in both dry years, again underlining the fact that atmospheric drivers control evaporation. In 2015, the high amount of precipitation in spring is reflected as a substantial rise in primary production, i.e., negative net ecosystem exchange. This surplus of GPP in spring coincides with reports in Bastos et al. (2020a), Smith et al. (2020) across Europe. This episode is followed by below-average carbon assimilation in the second half of 2015 (and 2018) as a result of the dry-down in soil water below a critical amount.

With regard to a categorization of DH1518 conditions, we highlighted the year 2016 for all variables shown in Fig. 5, which is used as a reference for normal conditions.

After the above discussion on the seasonal pattern of hydrological conditions as well as their impact on NEE, we now focus on the implication of the site management, i.e., grass cutting, for gross primary production under dry conditions (Fig. 6). The course of NEE and how it is partitioned into GPP and R_{eco} is shown in Fig. 6 for DH1518. GPP decreases dramatically after cutting events, with daily values close to zero in some cases. This effect is more pronounced at the considered observation site Büel-Rietholzbach compared to other sites in Switzerland,

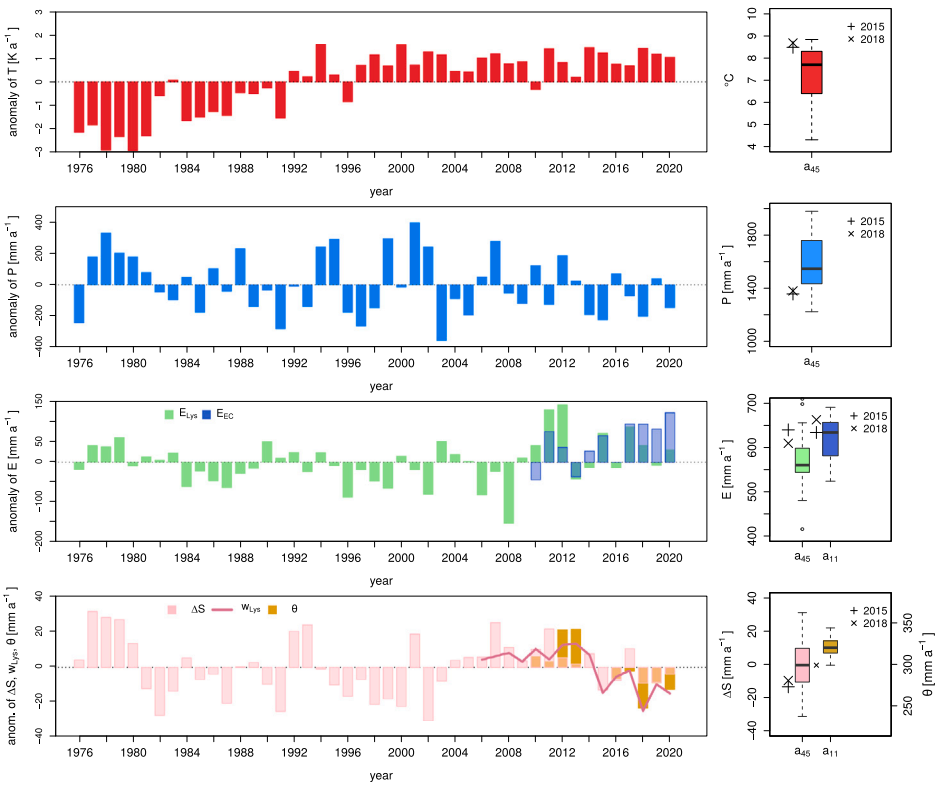

Fig. 4. *Left panels:* Annual anomalies of temperature (top), precipitation (second to top), evapotranspiration (second to bottom) and soil water content (bottom), wrt. the long-term mean of the available data series, i.e., 45 years in the case of T, P, E_{Lys} and ΔS. In the case of E_{EC} the anomalies are calculated wrt. the long-term-mean of E_{Lys}. For θ and w_{Lys} the mean is based on 11 and 15 years, respectively. w_{Lys} refers to the annual anomalies of lysimeter weight-based measurements, i.e., water storage changes. The brown bars in the same panel denote WCR-based data since 2010. For this series, annual totals from 2014 and 2015 are missing, due to missing data in those years. *Right panels*: Distribution of the available data since 1976 (a_{45}) including the dry years DH1518. The colored bar denotes the inter-quartile range, the dashed vertical lines denote the 5% to 95% range. The dry years are highlighted with a cross and a plus sign. (For interpretation of the references to color in this figure legend, the reader is referred to the web version of this article.)

as mentioned, e.g., in Wolf et al. (2014). The distinct drop in primary production is related to the applied cutting practice, i.e., how much of the biomass is removed. In the case of Büel-Rietholzbach, the grass is cut very close to the surface, and only a short stubble is left, shutting down GPP almost entirely.

Evapotranspiration, on the other hand, shows no clear response to cutting events, although transpiration is expected to be dramatically reduced. We assume that increased soil evaporation due to higher exposure to solar radiation is compensating the reduction of transpiration after removing the vegetation. As mentioned above, the soil water storage is able to sustain the water supply for evaporation even during the dry periods. The resilience of E to dry atmospheric conditions at this location is underlined with the Priestley–Taylor evaporation. The Priestley–Taylor equation calculates E_{PT} as function of the available energy, the slope of the saturation vapor density curve and the psychrometric constant only, see Eq. (4). In Fig. 6, we used the empirical coefficient $\alpha = 1.26$ for saturated surfaces, i.e., potential evaporation (Priestley and Taylor, 1972). It is apparent, that E closely follows the energy-driven E_{PT}, even under dry conditions. There is, however, a tendency towards lower actual E during the summer of 2018.

In terms of the water use efficiency index (WUE), which describes how efficient water is used for carbon assimilation, this decorrelation of GPP and E results in a substantial decrease of WUE in the days after a cutting event (Fig. 8), as the water is vastly used in evaporation instead of biomass production. Taking grass cutting into account when deriving hydrological indices such as WUE can be of great importance for characterizing responses of land–atmosphere systems to a changing climate. Fig. 7 highlights the effect of dryness in DH1518 on GPP in with respect to the range of all other years since 2010. The signal of cutting is clearly visible in the average annual course for all normal and dry years as distinct drops around the two first cutting events per growing season in May/June and June/July (Fig. 2), as mentioned in Section 2.2. Still, in DH1518 the attenuation of primary production in summer as a consequence of the water deficit is clearly visible for both years. The effect lasts as long as the end of the main growing season end of October, when GPP reaches average values again and is correlated to the soil water storage shown in Fig. 5. The surplus of GPP in 2015 compared to the other years as a result of a wet spring allows GPP to sustain a relatively high level until the dry conditions take effect in July. Overall, the annual deficit of gross primary production in DH1518, that was reported in different studies (Bastos et al., 2020a; Fu et al., 2020; Smith et al., 2020) is intensified at the Büel-Rietholzbach site due to the rigorous cutting at the site Büel-Rietholzbach, which inhibits a full recovery of biomass production under the dry conditions.

We performed a superposed epoch analysis to help understand and visualize the impact of cutting on biomass production under normal and dry conditions at the site Büel-Rietholzbach. The emerging patterns of GPP, E_{EC}, WUE and R_{eco} in the days before and after a cutting event are demonstrated in Fig. 8. The distinct drop in GPP after cutting is clearly detectable for both normal and dry conditions, as carbon assimilating biomass is removed. Note that the minimum of GPP is usually not reached immediately after the cut, but rather three days later, on average. This might be related to an uncertainty between the modeled daytime R_{eco} and measured NEE in the days following the cutting, when the carbon sink efficiency is reduced, while CO_2 is released due to heterotrophic respiration. In general, the cut grass is left to dry on the field. It may also be surprising that GPP is often highest not right before the cut, but rather some days earlier. This relates to the fact that the cutting often takes place after rain events, i.e., at the beginning of dry periods. During the rainy events prior to the cutting GPP is lower due to reduced photosynthetic activity. From

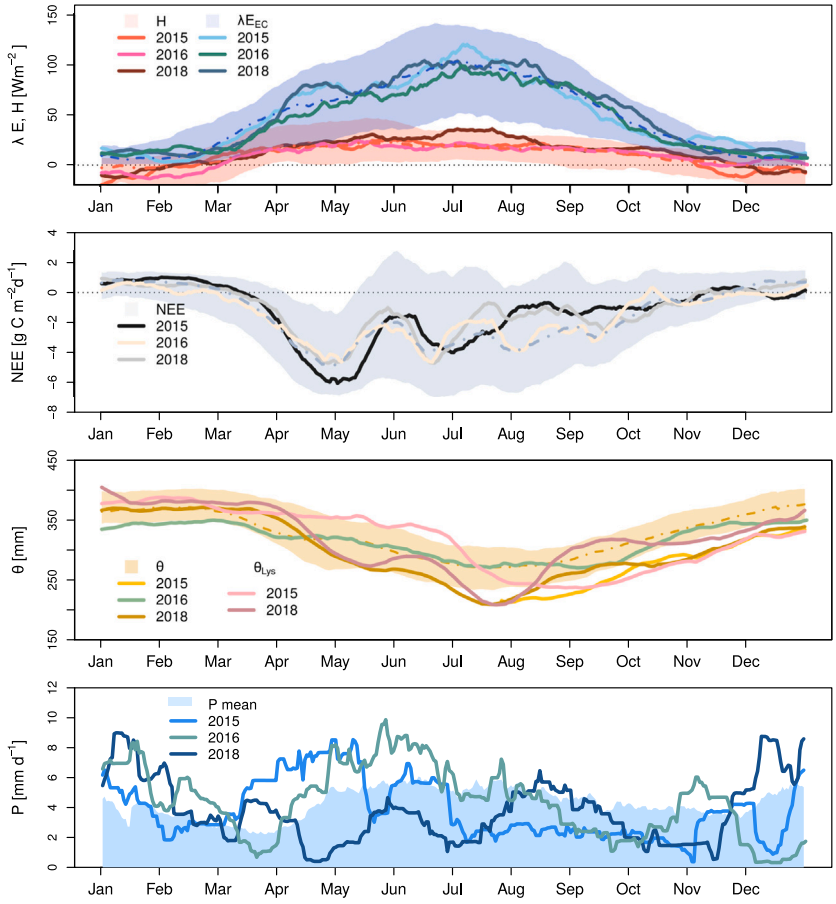

Fig. 5. Seasonal pattern of daily sensible heat H and latent heat flux λE_{EC} (top), net ecosystem exchange NEE (second to top) and daily soil water content θ (second to bottom) from 2010 to 2020 without DH1518. The shaded area denotes the 5% to 95% range, the dashed lines represent the median. In the bottom panel the shaded area is the average daily precipitation. The dry years 2015 and 2018 as well as the 'normal' year 2016 are shown separately (solid lines). For θ in DH1518 apart from the CS616-measured data also the lysimeter-based soil moisture data (θ_{Lys}) are shown. Data are smoothed with a 31-day running mean.

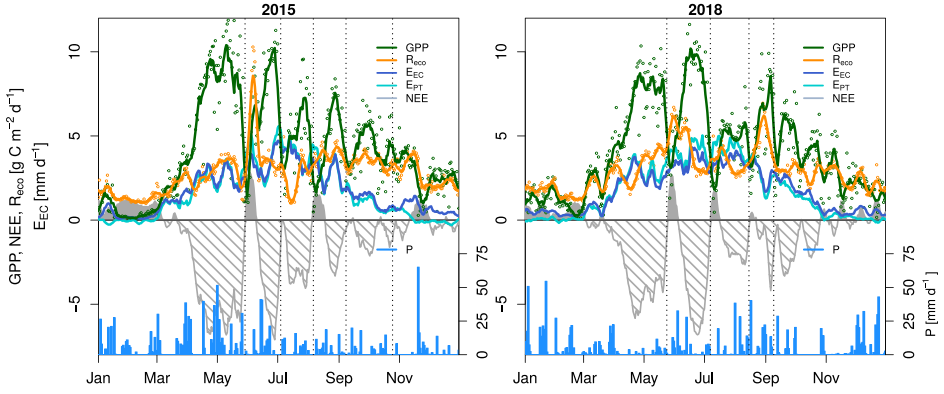

Fig. 6. Gross primary production (GPP), ecosystem respiration (R_{eco}), net ecosystem exchange (NEE), EC-observed evapotranspiration (E_{EC}), potential evaporation (E_{PT}) and precipitation (P) at the Büel-Rietholzbach research site in the dry years 2015 and 2018. Dots and bars denote daily data, solid lines represent the 7-day running mean. The vertical dotted lines denote cutting events.

the emerging pattern of normalized GPP after cutting, we infer that after 21 days, on average, the primary production rates are equal to the case before cutting. We consider the time period from 10 days prior to the cutting until 21 days after as the period, during which GPP is substantially attenuated due to the cutting. Additionally, we assume that the effect of cutting during that time outweighs meteorological effects.

As shown earlier, E is not significantly affected by the loss of vegetation on average, as soil evaporation compensates for the decrease in transpiration. Consequently, as water is lost to the atmosphere via evaporation and cannot be used for photosynthesis, the water use efficiency is substantially declining along with GPP.

In order to quantitatively disentangle cutting effects from meteorological effects on GPP, the measured time series is compared to the version minus the cutting effect (GPP_{nc}) as well as the idealized undistorted climatology (GPP_{95}), see Fig. 9. The observed GPP in DH1518 is plotted against GPP_{95} and the mean of daily GPP to reveal the impact of meteorological and hydrological effects on primary production. The

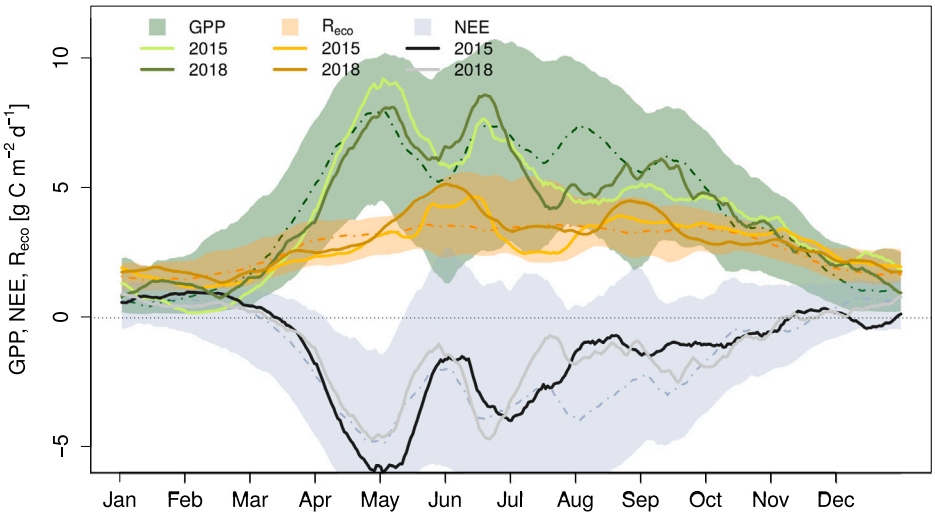

Fig. 7. Inter-annual variability of daily gross primary production (GPP), net ecosystem exchange (NEE) and ecosystem respiration (R_{eco}) from 2010 until 2020 without DH1518. The shaded area denotes the 5% to 95% range, the dashed lines represent the median. The dry years 2015 and 2018 are shown separately (solid lines). Data are smoothed with a 31-day running mean.

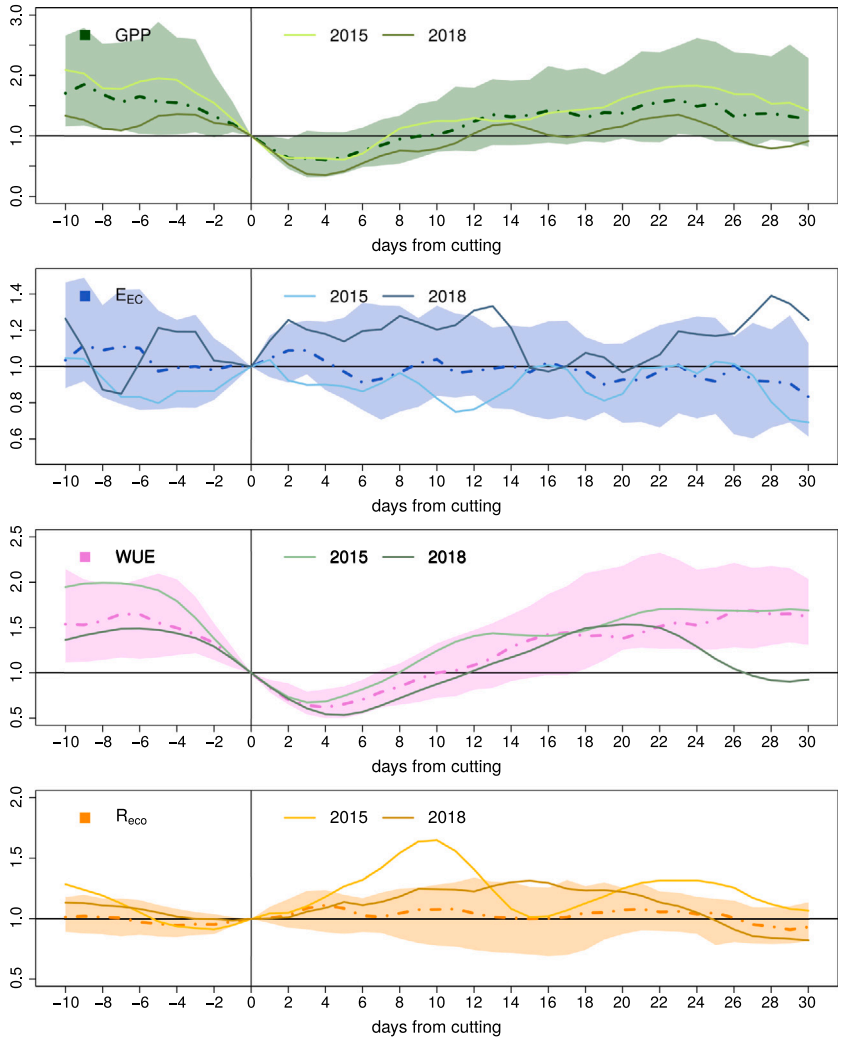

Fig. 8. Superposed epoch analysis of daily normalized gross primary production GPP, evapotranspiration E_{EC} and water use efficiency $WUE = GPP/E_{EC}$ before and after cutting. Shown are 10 days prior and 30 days after each of the 48 cutting events. The actual cutting day is positioned at zero. The data are normalized with the respective amount at the cutting day. The shaded are denotes the 25% to 75% range, the solid lines represent the median. The data are smoothed with a 3-day running mean.

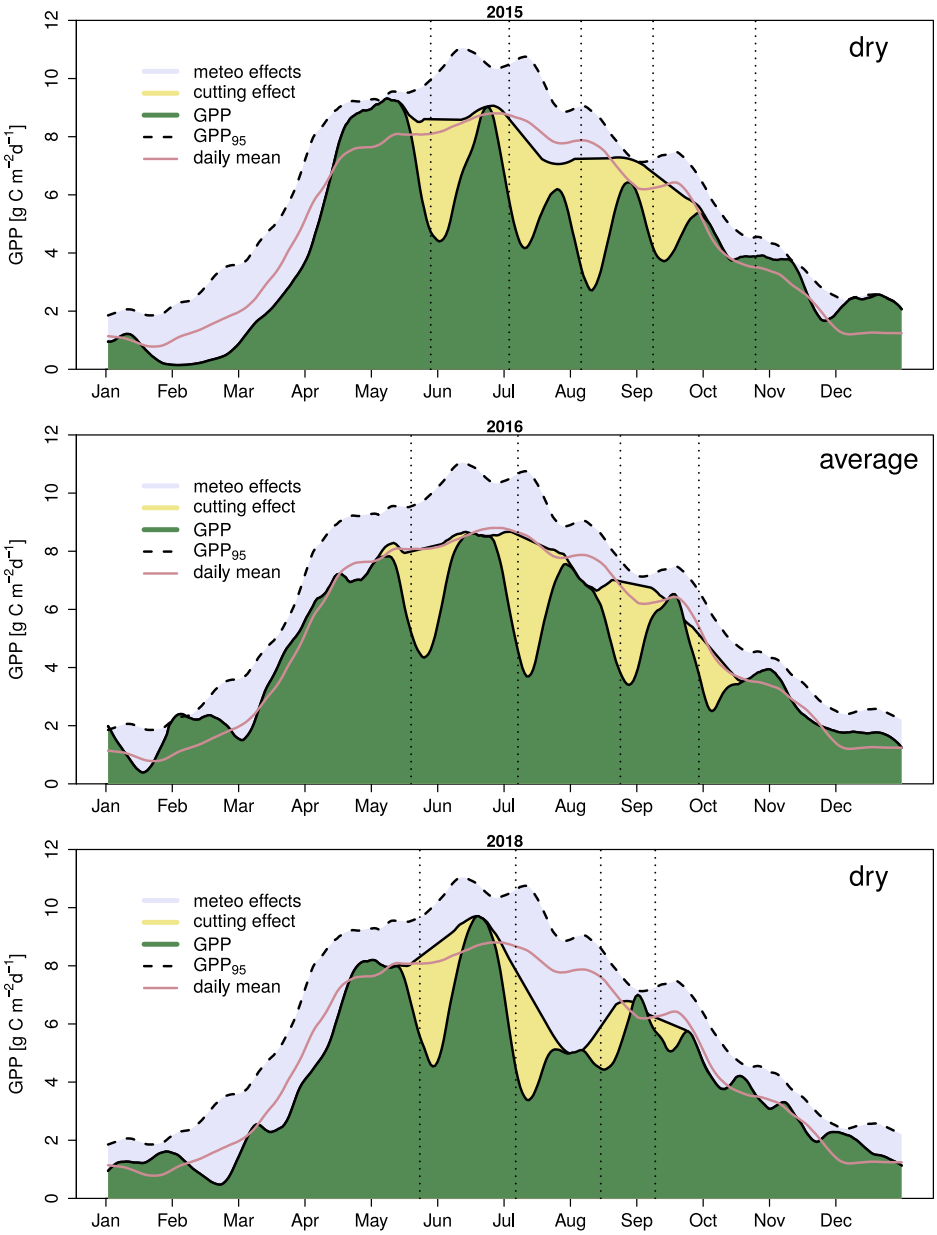

Fig. 9. Seasonal evolution of GPP_{95} and observed GPP in the average year 2016 and the dry years DH1518. The red line denotes the daily mean of GPP from 2010 to 2020 (without DH1518) with eliminated effect of cutting (green area plus yellow area). The dotted vertical lines denote cutting events. (For interpretation of the references to color in this figure legend, the reader is referred to the web version of this article.)

difference between GPP_{nc} and original GPP then accounts for the influence of cutting the grass. For both dry years it becomes apparent that GPP was substantially decreased in comparison to GPP_{95} after the second cutting in July, when soil moisture was distinctively lower than average in both cases. The propagation of GPP in both years differs as function of precipitation, see Fig. 5. The year 2015 was rather wet in the first half of the year, followed by a consistently increasing water deficit in the second half of summer. The second cutting event in July thus had a large impact on GPP, as the vegetation could not fully recover afterwards in the dry conditions, which is indicated as a consistent decline in GPP after the second cutting. The year 2018 was already dry in spring and water availability almost constantly below average. However, GPP seems unaffected by this in the first half of the year. The even more distinct precipitation and soil water deficit in July, however, which also coincided with a cutting event, led to a substantial deficit in GPP by the end of the year. This is in contrast to the evolution of GPP in 2016, which was an average year in terms of meteorological conditions, i.e., soil moisture, and primary production, see Fig. 5 and Table 2. In this case, GPP swiftly recovers after a cutting event to the average level at the respective time of the year.

When the effect of cutting is corrected (see GPP_{nc} in Table 2), among DH1518 only 2018 stands out as a year with a pronounced deficit in primary production. The rate of GPP after cutting seems to be substantially more diminished in the dry conditions observed in the second half of 2018, compared to the effect of the dry conditions on GPP in 2015. It remains elusive from this analysis, whether the seasonal evolution of GPP in 2015 would have been nearly average without the cutting. The 2018 GPP deficit, in contrast, was most likely to a great extent a result of the drought period and severe plant drought stress (Bastos et al., 2020a), albeit strongly intensified by cutting. The years 2010 and 2013 stand out with relatively high anomalies in the case of GPP_{nc}. This deficit is explained by a comparably slow and late start of the growing season (not shown). Conversely, the high anomaly of annual GPP in 2017 and especially 2020 is a result of the very early

Table 2
Annual sums and anomalies of gross primary production (GPP). Sums are given in kg C $m^{-2}a^{-1}$ and anomalies are given in percent wrt. the overall mean without DH1518. The subscript nc indicates the case where the effects of grass cutting have been removed. The annual sum of GPP_{95} is 2.293 kg C m^{-2}.

Year	GPP	GPP_{nc}	Rel. anomaly	Rel. anomaly$_{nc}$
2010	1.419	1.580	−20.3	−11.3
2011	1.651	1.710	−7.3	−4.0
2012	1.475	1.697	−17.2	−4.7
2013	1.339	1.496	−24.8	−16.0
2014	1.733	2.054	−2.7	15.4
2015	1.491	1.772	−16.3	−0.5
2016	1.578	1.819	−11.4	2.1
2017	1.644	1.988	−7.7	11.6
2018	1.514	1.684	−15.0	−5.5
2019	1.586	1.839	−11.0	3.3
2020	1.621	1.845	−9.0	3.6
Mean	1.550	1.771		

start of the growing season, which is reflected, at least for 2017, in the early first cutting event in Fig. 2.

4. Conclusions

In this study we have presented and analyzed eddy-covariance flux measurements of sensible heat flux, latent heat flux, and net ecosystem exchange at a pre-alpine research site in temperate humid conditions. We have focused on the impact of dry conditions on the gross primary production of the managed grassland around the research site. In addition, we have evaluated the use of a standardized processing scheme and compared it to a previously used processing scheme.

We identified at the presented site in Switzerland that managing a grassland crop, i.e., cutting the grass when it has reached maturity, has a major reducing impact on observed GPP on a short-term scale of several days but also on annual total production. This effect is enhanced in dry conditions, such as the drought events in 2015 and 2018, when the GPP deficit persists for the entire growing period. This can be of importance if the measured net ecosystem exchange of CO_2 is used to characterize a site by its sink potential or water use efficiency. We have also introduced a simple way of disentangling and quantifying the effects of cutting and dryness on biomass production. This revealed that while the 2015 drought was of similar amplitude as the one in 2018, the annual GPP deficit in 2015 at the site Büel-Rietholzbach was more strongly affected by grass cutting than from vegetation drought stress. It is not clear, however, to what extent the variability of cutting-depth, i.e., how much of the biomass is removed, plays a role in the inter-annual differences of total GPP. The rather wet conditions in spring (2015) and early summer (2018) in the considered two dry years resulted in an increased growth prior to the dry spells, consistent with results from (Bastos et al., 2020a; Smith et al., 2020). This surplus of primary production mitigated the deficit of total annual GPP in both years to some extent in comparison to other years. Evapotranspiration, in contrast, was not significantly affected by these dry periods, indicating that the reduced soil water storage was not a limiting factor for evapotranspiration at this humid location due to the ample water availability. This underlines a stronger resilience to drought events in Switzerland to some degree in comparison to, e.g., the Mediterranean region, where water availability is constrained more substantially by precipitation. Consequently, water use efficiency was diminished during the dry periods.

The effect of management is substantial at the presented research site due to the way the grass is cut, but may vary at other sites. Persistent water deficits during droughts substantially intensify the impact of grass cutting by prolonging the recovery period.

With regard to an analysis of different sites in a network such as FLUXNET (Baldocchi et al., 2001) or Swiss FluxNet (http://www.swissfluxnet.ch) these findings can help to homogenize the results between managed and non-managed grassland sites, which would help assess more robustly the responses of the environment to droughts and global warming.

With regard to the eddy-covariance flux calculation in the previously used and the current processing scheme we conclude that the differences between the data sets can be substantial, but are always traceable and related to fundamental changes in how the data are treated. The most important changes between the previously used and current processing scheme are the length of the averaging interval (30 min instead of 60 min), linear detrending the rawdata prior to averaging instead of no detrending and the gap-filling procedures (e.g., look-up table instead of linear regression), as well as performing the tests for stationarity and well-developed turbulence. Also, all EC measurements, i.e., λE_{EC}, H and NEE during rain events are discarded and gap-filled in the current scheme instead of set to zero in the case of λE_{EC}. The differences between the resulting datasets do not allow for a seamless continuation of the EC data series with the new processing scheme. The current processing scheme is rather used to re-process the rawdata to produce an alternate time series, which will serve as the standard data series of EC fluxes from this research site.

Declaration of competing interest

One or more of the authors of this paper have disclosed potential or pertinent conflicts of interest, which may include receipt of payment, either direct or indirect, institutional support, or association with an entity in the biomedical field which may be perceived to have potential conflict of interest with this work. For full disclosure statements refer to https://doi.org/10.1016/j.agrformet.2022.109166. Dominik Michel reports financial support was provided by GCOS Switzerland.

Acknowledgment

We acknowledge financial support from GCOS Switzerland through the SMiLE-ECV-CH project.

Appendix A. u_*-filtering

The eddy-covariance method requires a certain amount of turbulence intensity in order to work. NEE measurements, for instance, tend to be underestimated when turbulence intensity is at the lower end of the site-specific distribution of u_*, which often occurs in stable stratification during the night. Nighttime fluxes were classified as unreliable and discarded, when u_* falls below an annually estimated threshold. The threshold was determined based on the relation of NEE and u_* within temperature subsets (Papale et al., 2006). The uncertainty of the detection method was assessed applying a bootstrapping method 100 times on the measured u_* (Efron and Tibshirani, 1986). The respective median of the bootstrapping result was used as the u_* threshold in a specific year. The thresholds for 2010–2020 range from 0.03 to 0.05 ms^{-1}. The mean daytime shear stress velocity is 0.16 ms^{-1}.

Appendix B. Gap-filling performance

As the bin size is increased in search of measured fluxes to replace the missing value in the MDS method, different quality flags are assigned to the replaced value. In this study, quality flag A.1 is used for cases with R_{sd}, T and VPD available within a ±7 day window. Quality flag A is used if either LUT is applied with a window of up to ±14 days (R_{sd}, T and VPD available), ±7 days (R_{sd} available) or MDC within ±1 h. Quality flag B denotes cases, where either LUT is applied with a bin size of ±28 days (R_{sd}, T and VPD available), ±14 days (R_{sd} available) or MDC within ±1 day, respectively. All further increases of the window size in the respective method are assigned with label C (not shown). Only gaps with a length up to 60 days are filled.

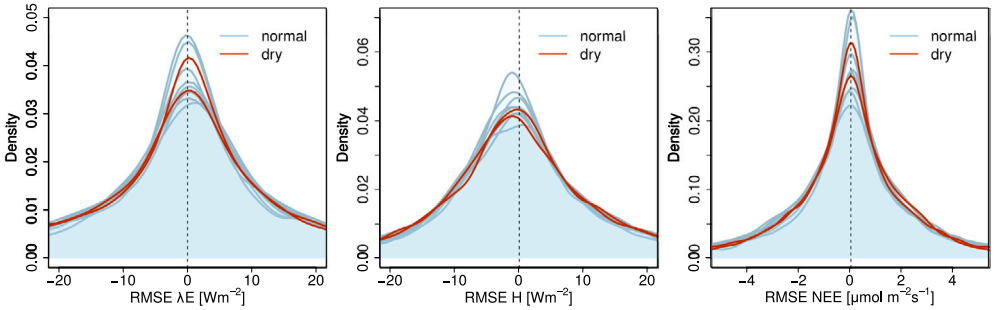

Fig. B.10. Annual distribution of the root mean square error (RMSE) between original and gap-filled data with marginal distribution sampling (MDS). Highlighted are the dry years 2015 and 2018.

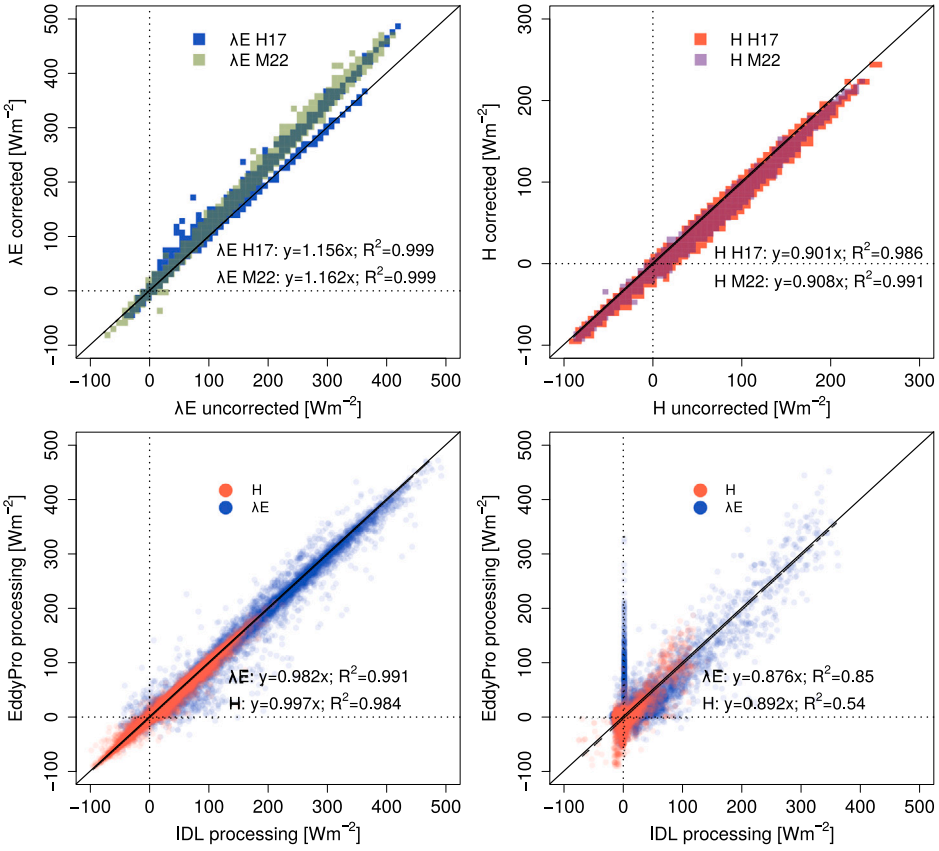

Fig. C.11. Sensible and latent heat fluxes based on present processing scheme involving EddyPro versus processing scheme used in H17. *Top panels*: Comparison of the influence of eddy covariance corrections to calculated the latent and sensible heat flux in the current processing scheme M22 and previous processing scheme H17. *Bottom left*: Correlation of calculated heat fluxes based on direct measurements only. *Bottom right*: Correlation of calculated heat fluxes based on gap-filled data only.

Meteorological data used for the gap-filling-algorithm were measured at the Büel-Rietholzbach site (Section 2.5). Fig. 3 shows that the large majority (≤95%) of the gaps in all time series could be filled applying the LUT approach with adjacent data within ±7 days of the missing values (quality flag A.1). With data within a maximum window of 14 days (quality flag A) more than 96% of the gaps are filled and with a maximum window of ±28 days (quality flag B) more than 99% are reached. The remaining < 1% of the gaps is filled with quality flag C values.

The performance of the gap-filling procedure on the three half-hourly datasets λE, H and NEE is also shown in Fig. 3, where original measurements are compared to their MDS-based estimates. Note that for quality flag C there are no original values available to test the gapfilling performance. There is no apparent difference of uncertainty between the two gap-filling classes. This comparison, however, is not significant with regard to the small sample size of flag B. The root mean square error (RMSE) of the MDS-estimated data for DH1518 is 24.4 Wm^{-2} for λE, 14.6 Wm^{-2} for H and 3.1 µmol m^{-2}s^{-1} for NEE. In the case of the normal year sample the respective RMSE is 24.5 and 14.3 Wm^{-2} and 3.2 µmol m^{-2}s^{-1}. The similarity of the RMSE values for dry and normal conditions indicates that there is no bias in the gap-filling procedure due to variability in meteorological conditions, which could distort the correlation of normal to dry years in this study. The annual distributions of the RMSE of gapfilled data are shown in Fig. B.10.

Appendix C. Consistency of H and λE processing with earlier versions

While the H17 and M22 data sets are both based on the same raw data, they are independent products. Only in M22 we present CO_2 data from the Büel-Rietholzbach research site. The derived fluxes can substantially deviate in some cases, as different processing steps

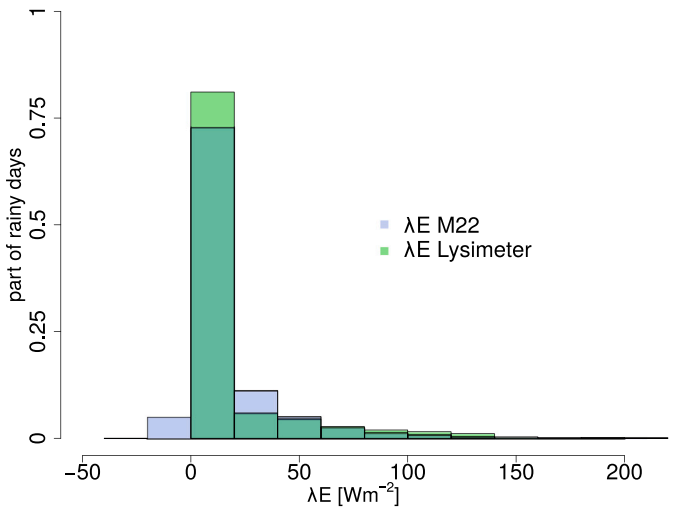

Fig. C.12. Frequency and magnitude of λE during rainy hours from gap-filled EC measurements and as observed by the lysimeter in the period 2009 to 2015. Note that the lysimeter only provides positive values.

are involved on the way to the final product. The discrepancies originate mainly from (a) calculating the covariance matrix, (b) the flux correction procedure, and (c) the gap-filling procedure.

As the used EC raw data and flux correction sequences do not fundamentally differ, the changes from uncorrected to corrected fluxes are very similar in both H17 and M22. Fig. C.11 shows that the flux correction procedures essentially act in the same way in both data processing schemes. The present M22 data have been aggregated from half-hourly to hourly values for this analysis. λE is increased by around 15% and H is reduced by approximately 10% after correction, as indicated by the regression slope. These substantial effects mainly result from the spectral correction for sensor separation in the case of λE and the conversion of the buoyancy flux in the case of H. The apparent difference between H17 and M22 is that while the EddyPro processing corrects all data in a consistent fashion, certain few instances of λE are only marginally changed in the H17 processing (i.e., the data stay on the 1:1 line). This is due to the different spectral correction methods used (Moore, 1986; Moncrieff et al., 2005), which act differently as function of wind speed.

The comparison of the two different corrected flux series (bottom panels in Fig. C.11) reveals a substantial spread of the data, while the correlation is strong, as expected. The spread is explained mostly by the different averaging methods. In M22 linear detrending of flux components is performed within half-hourly windows for decomposing them into mean and turbulent parts prior to calculating the covariances. In the case of H17, no detrending is performed within hourly windows. This can lead to over- or underestimation of the covariances especially in H17, when a trend in the data, e.g., a temperature increase, affects the magnitude of the turbulent fluctuations of T. For reference, detrending the flux components and using half hourly data instead of using the average of hourly values results in an overall difference, expressed as RMSE, of 11.3 Wm^{-2} (3.4 Wm^{-2} in the 5 to 95% range) in the case of λE and 4.8 Wm^{-2} (2.1 Wm^{-2} in the 5 to 95% range) in the case of H.

In general, though, larger deviations between the final flux series of H17 and M22 result from gap-filling, as H17 relies on interpolation and a regression with solar radiation (Hirschi et al., 2017) in the case of λE, which fundamentally differs from the MDS approach used in M22. Fig. C.11 shows that the correlation of the gap-filled data is still relatively high (R^2 of 0.85 and 0.54 for λE and H, respectively). Overall, the EddyPro gap-filled data are around 12% lower than the H17 gap-filled data. Note that the statistical metrics for λE are calculated without rainy hours, because rainy hours are handled differently in H17 and M22. In H17 these values are replaced with zero and in M22 these values are discarded and replaced with MDS, which does not take into account whether it rains or not. While assuming E to be zero during rain as in H17 is physically sound, measurements of E with the lysimeter during rain still indicate a substantial amount of evaporation occurring. This has also been reported in Hirschi et al. (2017). Fig. C.12 shows that in light of the lysimeter measurements the magnitude of λE during rain modeled by MDS is reasonable, with the majority being below 25 Wm^{-2}.

References

BAFU (Ed.), 2016. Hitze Und Trockenheit Im Sommer 2015. Auswirkungen Auf Mensch und Umwelt. Umwelt-Zustand Nr. 1629, Bundesamt für Umwelt BAFU, Bern, p. 108.

BAFU, et al. (Eds.), 2019. Hitze und Trockenheit im Sommer 2018. Auswirkungen auf Mensch und Umwelt. Umwelt-Zustand Nr. 1909, Bundesamt für Umwelt, Bern, p. 91.

Baldocchi, D., Falge, E., Gu, L., Olson, R., Hollinger, D., Running, S., Anthoni, P., Bernhofer, C., Davis, K., Evans, R., Fuentes, J., Goldstein, A., Katul, G., Law, B., Lee, X., Malhi, Y., Meyers, T., Munger, W., Oechel, W., Paw U, K., Pilegaard, K., Schmid, H.P., Valentini, R., Verma, S., Vesala, T., Wilson, K., Wofsy, S., 2001. FLUXNET: A new tool to study the temporal and spatial variability of ecosystem-scale carbon dioxide, water vapor, and energy flux densities. Bull. Am. Meteorol. Soc. 82 (11), 2415–2434. http://dx.doi.org/10.1175/1520-0477(2001)082<2415:FANTTS>2.3.CO;2.

Bastos, A., Ciais, P., Friedlingstein, P., Sitch, S., Pongratz, J., Fan, L., Wigneron, J.P., Weber, U., Reichstein, M., Fu, Z., Anthoni, P., Arneth, A., Haverd, V., Jain, A.K., Joetzjer, E., Knauer, J., Lienert, S., Loughran, T., McGuire, P.C., Tian, H., Viovy, N., Zaehle, S., 2020a. Direct and seasonal legacy effects of the 2018 heat wave and drought on European ecosystem productivity. Sci. Adv. 6 (24), http://dx.doi.org/10.1126/sciadv.aba2724, URL: https://advances.sciencemag.org/content/6/24/eaba2724.

Bastos, A., Fu, Z., Ciais, P., Friedlingstein, P., Sitch, S., Pongratz, J., Weber, U., Reichstein, M., Anthoni, P., Arneth, A., Haverd, V., Jain, A., Joetzjer, E., Knauer, J., Lienert, S., Loughran, T., McGuire, P.C., Obermeier, W., Padrón, R.S., Shi, H., Tian, H., Viovy, N., Zaehle, S., 2020b. Impacts of extreme summers on European ecosystems: A comparative analysis of 2003, 2010 and 2018. Philos. Trans. R. Soc. B 375 (1810), 20190507. http://dx.doi.org/10.1098/rstb.2019.0507, URL: https://royalsocietypublishing.org/doi/abs/10.1098/rstb.2019.0507.

Buras, A., Rammig, A., Zang, C.S., 2020. Quantifying impacts of the 2018 drought on European ecosystems in comparison to 2003. Biogeosciences 17 (6), 1655–1672. http://dx.doi.org/10.5194/bg-17-1655-2020, URL: https://bg.copernicus.org/articles/17/1655/2020/.

Dong, B., Sutton, R., Shaffrey, L., Wilcox, L., 2017. The 2015 European heat wave. Bull. Am. Meteorol. Soc. 97 (12), S57–S62. http://dx.doi.org/10.1175/BAMS-D-16-0140.1.

Efron, B., Tibshirani, R., 1986. Bootstrap methods for standard errors, confidence intervals, and other measures of statistical accuracy. Statist. Sci. 1 (1), 54–75. http://dx.doi.org/10.1214/ss/1177013815.

Fink, A.H., Brücher, T., Krüger, A., Leckebusch, G.C., Pinto, J.G., Ulbrich, U., 2004. The 2003 European summer heatwaves and drought –Synoptic diagnosis and impacts. Weather 59 (8), 209–216. http://dx.doi.org/10.1256/wea.73.04, URL: https://rmets.onlinelibrary.wiley.com/doi/abs/10.1256/wea.73.04.

Foken, T., Wichura, B., 1996. Tools for quality assessment of surface-based flux measurements. Agricult. Forest Meteorol. 78 (1), 83–105. http://dx.doi.org/10.1016/0168-1923(95)02248-1, URL: https://www.sciencedirect.com/science/article/pii/0168192395022481.

Fu, Z., Ciais, P., Bastos, A., Stoy, P.C., Yang, H., Green, J.K., Wang, B., Yu, K., Huang, Y., Knohl, A., Šigut, L., Gharun, M., Cuntz, M., Arriga, N., Roland, M., Peichl, M., Migliavacca, M., Cremonese, E., Varlagin, A., Brümmer, C., Gourlez de la Motte, L., Fares, S., Buchmann, N., El-Madany, T.S., Pitacco, A., Vendrame, N., Li, Z., Vincke, C., Magliulo, E., Koebsch, F., 2020. Sensitivity of gross primary productivity to climatic drivers during the summer drought of 2018 in Europe. Philos. Trans. R. Soc. B 375 (1810), http://dx.doi.org/10.1098/rstb.2019.0747, URL: https://royalsocietypublishing.org/doi/abs/10.1098/rstb.2019.0747.

García-Herrera, R., Díaz, J., Trigo, R.M., Luterbacher, J., Fischer, E.M., 2010. A review of the European summer heat wave of 2003. Crit. Rev. Environ. Sci. Technol. 40 (4), 267–306. http://dx.doi.org/10.1080/10643380802238137.

Gharun, M., Hörtnagl, L., Paul-Limoges, E., Ghiasi, S., Feigenwinter, I., Burri, S., Marquardt, K., Etzold, S., Zweifel, R., Eugster, W., Buchmann, N., 2020. Physiological response of swiss ecosystems to 2018 drought across plant types and elevation. Philos. Trans. R. Soc. B 375 (1810), 20190521. http://dx.doi.org/10.1098/rstb.2019.0521, URL: https://royalsocietypublishing.org/doi/abs/10.1098/rstb.2019.0521.

Gurtz, J., Badertscher, S., Milzow, C., Moser, U., Schroff, K., Stoeckli, R., Völksch, M., 2006. Analysis of the Time Series of Meteorological and Hydrological Measurements in the Rietholzbach Research Catchment Between 1976 and 2005 with Special Consideration of the Dry Summer 2003. Technical Report, ETH Zurich, Zurich, Switzerland.

Gurtz, J., Verbunt, M., Zappa, M., Moesch, M., Pos, F., Moser, U., 2003. Long-term hydrometeorological measurements and model-based analyses in the hydrological research catchment Rietholzbach. J. Hydrol. Hydromech. 51 (3), 162–174, URL: http://dlib.lib.cas.cz/4634/.

Hanel, M., Rakovec, O., Markonis, Y., Máca, P., Samaniego, L., Kyselý, J., Kumar, R., 2018. Revisiting the recent European droughts from a long-term perspective. Sci. Rep. 8 (9499), http://dx.doi.org/10.1038/s41598-018-27464-4.

Hari, V., Rakovec, O., Markonis, Y., Hanel, M., Kumar, R., 2020. Increased future occurrences of the exceptional 2018–2019 central European drought under global warming. Sci. Rep. 10 (12207), http://dx.doi.org/10.1038/s41598-020-68872-9.

Hauser, M., Gudmundsson, L., Orth, R., Jézéquel, A., Haustein, K., Vautard, R., van Oldenborgh, G.J., Wilcox, L., Seneviratne, S.I., 2017. Methods and model dependency of extreme event attribution: The 2015 European drought. Earth's Future 5 (10), 1034–1043. http://dx.doi.org/10.1002/2017EF000612, URL: https://agupubs.onlinelibrary.wiley.com/doi/abs/10.1002/2017EF000612.

Hirschi, M., Michel, D., Lehner, I., Seneviratne, S.I., 2017. A site-level comparison of lysimeter and eddy covariance flux measurements of evapotranspiration. Hydrol. Earth Syst. Sci. 21 (3), 1809–1825. http://dx.doi.org/10.5194/hess-21-1809-2017, URL: https://www.hydrol-earth-syst-sci.net/21/1809/2017/.

Ionita, M., Tallaksen, L.M., Kingston, D.G., Stagge, J.H., Laaha, G., Van Lanen, H.A.J., Scholz, P., Chelcea, S.M., Haslinger, K., 2017. The European 2015 drought from a climatological perspective. Hydrol. Earth Syst. Sci. 21 (3), 1397–1419. http://dx.doi.org/10.5194/hess-21-1397-2017, URL: https://hess.copernicus.org/articles/21/1397/2017/.

Liu, L., Gudmundsson, L., Hauser, M., Qin, D., Li, S., Seneviratne, S.I., 2020. Soil moisture dominates dryness stress on ecosystem production globally. Nature Commun. 11 (4892), http://dx.doi.org/10.1038/s41467-020-18631-1.

Lloyd, J., Taylor, J.A., 1994. On the temperature dependence of soil respiration. Funct. Ecol. 8 (3), 315–323, URL: http://www.jstor.org/stable/2389824.

Massman, W.J., 2000. A simple method for estimating frequency response corrections for eddy covariance systems. Agricult. Forest Meteorol. 104 (3), 185–198. http://dx.doi.org/10.1016/S0168-1923(00)00164-7, URL: http://www.sciencedirect.com/science/article/pii/S0168192300001647.

Massman, W.J., 2001. Reply to comment by rannik on "A simple method for estimating frequency response corrections for eddy covariance systems". Agricult. Forest Meteorol. 107 (3), 247–251. http://dx.doi.org/10.1016/S0168-1923(00)00237-9, URL: http://www.sciencedirect.com/science/article/pii/S0168192300002379.

Mauder, M., Foken, T., 2004. Documentation and Instruction Manual of the Eddy-Covariance Software Package TK3. Universität Bayreuth, Abteilung Mikrometeorologie, pp. 1–60.

Mittelbach, H., Seneviratne, S.I., 2012. A new perspective on the spatio-temporal variability of soil moisture: Temporal dynamics versus time-invariant contributions. Hydrol. Earth Syst. Sci. 16 (7), 2169–2179. http://dx.doi.org/10.5194/hess-16-2169-2012, URL: https://hess.copernicus.org/articles/16/2169/2012/.

Moesch, M., 2001. Investigations on Hydrological and Climatological Characteristics of the Research Catchment Rietholzbach. Technical Report, Inst. for Clim. Res., ETH Zurich, Zurich, Switzerland.

Moncrieff, J., Clément, R., Finnigan, J.J., Meyers, T., 2005. Averaging, detrending, and filtering of eddy covariance time series. In: Handbook of Micrometeorology. pp. 7–31.

Moore, C.J., 1986. Frequency response corrections for eddy correlation systems. Bound.-Lay. Meteorol. 37, 17–35.

Orth, R., Zscheischler, J., Seneviratne, S.I., 2016. Record dry summer in 2015 challenges precipitation projections in central Europe. Sci. Rep. 6 (28334), http://dx.doi.org/10.1038/srep28334.

Papale, D., Reichstein, M., Aubinet, M., Canfora, E., Bernhofer, C., Kutsch, W., Longdoz, B., Rambal, S., Valentini, R., Vesala, T., Yakir, D., 2006. Towards a standardized processing of net ecosystem exchange measured with eddy covariance technique: algorithms and uncertainty estimation. Biogeosciences 3 (4), 571–583. http://dx.doi.org/10.5194/bg-3-571-2006, URL: https://www.biogeosciences.net/3/571/2006/.

Priestley, C.H.B., Taylor, R.J., 1972. On the assessment of surface heat flux and evaporation using large-scale parameters. Mon. Weather Rev. 100 (2), 81–92. http://dx.doi.org/10.1175/1520-0493(1972)100<0081:OTAOSH>2.3.CO;2.

Ramonet, M., Ciais, P., Apadula, F., Bartyzel, J., Bastos, A., Bergamaschi, P., Blanc, P.E., Brunner, D., Caracciolo di Torchiarolo, L., Calzolari, F., Chen, H., Chmura, L., Colomb, A., Conil, S., Cristofanelli, P., Cuevas, E., Curcoll, R., Delmotte, M., di Sarra, A., Emmenegger, L., Forster, G., Frumau, A., Gerbig, C., Gheusi, F., Hammer, S., Haszpra, L., Hatakka, J., Hazan, L., Heliasz, M., Henne, S., Hensen, A., Hermansen, O., Keronen, P., Kivi, R., Komínková, K., Kubistin, D., Laurent, O., Laurila, T., Lavric, J.V., Lehner, I., Lehtinen, K.E.J., Leskinen, A., Leuenberger, M., Levin, I., Lindauer, M., Lopez, M., Myhre, C.L., Mammarella, I., Manca, G., Manning, A., Marek, M.V., Marklund, P., Martin, D., Meinhardt, F., Mihalopoulos, N., Mölder, M., Morgui, J.A., Necki, J., O'Doherty, S., O'Dowd, C., Ottosson, M., Philippon, C., Piacentino, S., Pichon, J.M., Plass-Duelmer, C., Resovsky, A., Rivier, L., Rodó, X., Sha, M.K., Scheeren, H.A., Sferlazzo, D., Spain, T.G., Stanley, K.M., Steinbacher, M., Trisolino, P., Vermeulen, A., Vítková, G., Weyrauch, D., Xueref-Remy, I., Yala, K., Yver Kwok, C., 2020. The fingerprint of the summer 2018 drought in Europe on ground-based atmospheric CO_2 measurements. Philos. Trans. R. Soc. B 375 (1810), http://dx.doi.org/10.1098/rstb.2019.0513, URL: https://royalsocietypublishing.org/doi/abs/10.1098/rstb.2019.0513.

Rassl, A., Michel, D., Hirschi, M., Duguay-Tetzlaff, A., Seneviratne, S.I., 2022. Climatological drought monitoring in Switzerland using EUMETSAT SAF satellite products. Remote Sens. (in revision).

Reichstein, M., Falge, E., Baldocchi, D., Papale, D., Aubinet, M., Berbigier, P., Bernhofer, C., Buchmann, N., Gilmanov, T., Granier, A., Grünwald, T., Havránková, K., Ilvesniemi, H., Janous, D., Knohl, A., Laurila, T., Lohila, A., Loustau, D., Matteucci, G., Meyers, T., Miglietta, F., Ourcival, J.-M., Pumpanen, J., Rambal, S., Rotenberg, E., Sanz, M., Tenhunen, J., Seufert, G., Vaccari, F., Vesala, T., Yakir, D., Valentini, R., 2005a. On the separation of net ecosystem exchange into assimilation and ecosystem respiration: Review and improved algorithm. Global Change Biol. 11 (9), 1424–1439. http://dx.doi.org/10.1111/j.1365-2486.2005.001002.x, URL: https://onlinelibrary.wiley.com/doi/abs/10.1111/j.1365-2486.2005.001002.x.

Reichstein, M., Kätterer, T., Andrén, O., Ciais, P., Schulze, E.-D., Cramer, W., Papale, D., Valentini, R., 2005b. Temperature sensitivity of decomposition in relation to soil organic matter pools: Critique and outlook. Biogeosciences 2 (4), 317–321. http://dx.doi.org/10.5194/bg-2-317-2005, URL: https://www.biogeosciences.net/2/317/2005/.

Reichstein, M., Subke, J.-A., Angeli, A.C., Tenhunen, J.D., 2005c. Does the temperature sensitivity of decomposition of soil organic matter depend upon water content, soil horizon, or incubation time? Global Change Biol. 11 (10), 1754–1767. http://dx.doi.org/10.1111/j.1365-2486.2005.001010.x, URL: https://onlinelibrary.wiley.com/doi/abs/10.1111/j.1365-2486.2005.001010.x.

Ruth, C., Michel, D., Hirschi, M., Seneviratne, S.I., 2018. Comparative study of a long-established large weighing lysimeter and a state-of-the-art mini-lysimeter. Vadose Zone J. 17, http://dx.doi.org/10.2136/vzj2017.01.0026.

Schotanus, P., Nieuwstadt, F.T.M., De Bruin, H.A.R., 1983. Temperature measurement with a sonic anemometer and its application to heat and moisture fluxes. Bound.-Lay. Meteorol. 26 (1), 81–93. http://dx.doi.org/10.1007/BF00164332.

Schuldt, B., Buras, A., Arend, M., Vitasse, Y., Beierkuhnlein, C., Damm, A., Gharun, M., Grams, T.E., Hauck, M., Hajek, P., Hartmann, H., Hiltbrunner, E., Hoch, G., Holloway-Phillips, M., Körner, C., Larysch, E., Lübbe, T., Nelson, D.B., Rammig, A., Rigling, A., Rose, L., Ruehr, N.K., Schumann, K., Weiser, F., Werner, C., Wohlgemuth, T., Zang, C.S., Kahmen, A., 2020. A first assessment of the impact of the extreme 2018 summer drought on central European forests. Basic Appl. Ecol. 45, 86–103. http://dx.doi.org/10.1016/j.baae.2020.04.003, URL: http://www.sciencedirect.com/science/article/pii/S1439179120300414.

Seneviratne, S.I., Lehner, I., Gurtz, J., Teuling, A.J., Lang, H., Moser, U., Grebner, D., Menzel, L., Schroff, K., Vitvar, T., Zappa, M., 2012. Swiss prealpine Rietholzbach research catchment and lysimeter: 32 year time series and 2003 drought event. Water Resour. Res. 48 (6), http://dx.doi.org/10.1029/2011WR011749, URL: https://agupubs.onlinelibrary.wiley.com/doi/abs/10.1029/2011WR011749.

Seneviratne, S.I., Zhang, X., Adnan, M., Badi, W., Dereczynski, C., Di Luca, A., Ghosh, S., Iskandar, I., Kossin, J., Lewis, S., Otto, F., Pinto, I., Satoh, M., Vicente-Serrano, S., Wehner, M., Zhou, B., 2021. Weather and climate extreme events in a changing climate. In: Masson-Delmotte, V., Zhai, P., Pirani, A., Connors, S.L., Péan, C., Berger, S., Caud, N., Chen, Y., Goldfarb, L., Gomis, M.I., Huang, M., Leitzell, K., Lonnoy, E., Matthews, J.B.R., Maycock, T.K., Waterfield, T., Yelekçi, O., Yu, R., Zhou, B. (Eds.), Climate Change 2021: The Physical Science Basis. Contribution of Working Group I To the Sixth Assessment Report of the Intergovernmental Panel on Climate Change. Cambridge University Press, Cambridge, United Kingdom and New York, NY, USA, pp. 1513–1766. http://dx.doi.org/10.1017/9781009157896.013.

Sippel, S., Otto, F.E.L., Flach, M., van Oldenborgh, G.J., 2017. The role of anthropogenic warming in 2015 central European heat waves. Bull. Am. Meteorol. Soc. 97 (12), S51–S56. http://dx.doi.org/10.1175/BAMS-D-16-0150.1.

Smith, N.E., Kooijmans, L.M.J., Koren, G., van Schaik, E., van der Woude, A.M., Wanders, N., Ramonet, M., Xueref-Remy, I., Siebicke, L., Manca, G., Brümmer, C., Baker, I.T., Haynes, K.D., Luijkx, I.T., Peters, W., 2020. Spring enhancement and summer reduction in carbon uptake during the 2018 drought in northwestern Europe. Philos. Trans. R. Soc. B 375 (1810), 20190509. http://dx.doi.org/10.1098/rstb.2019.0509, URL: https://royalsocietypublishing.org/doi/abs/10.1098/rstb.2019.0509.

Stocker, B.D., Zscheischler, J., Keenan, T.F., Prentice, I.C., Seneviratne, S.I., Peñuelas, J., 2019. Drought impacts on terrestrial primary production underestimated by satellite monitoring. Nat. Geosci. 12 (1810), 264–270. http://dx.doi.org/10.1038/s41561-019-0318-6.

Thompson, R.L., Broquet, G., Gerbig, C., Koch, T., Lang, M., Monteil, G., Munassar, S., Nickless, A., Scholze, M., Ramonet, M., Karstens, U., van Schaik, E., Wu, Z., Rödenbeck, C., 2020. Changes in net ecosystem exchange over Europe during the 2018 drought based on atmospheric observations. Philos. Trans.

R. Soc. B 375 (1810), http://dx.doi.org/10.1098/rstb.2019.0512, URL: https://royalsocietypublishing.org/doi/abs/10.1098/rstb.2019.0512.

von Buttlar, J., Zscheischler, J., Rammig, A., Sippel, S., Reichstein, M., Knohl, A., Jung, M., Menzer, O., Arain, M.A., Buchmann, N., Cescatti, A., Gianelle, D., Kiely, G., Law, B.E., Magliulo, V., Margolis, H., McCaughey, H., Merbold, L., Migliavacca, M., Montagnani, L., Oechel, W., Pavelka, M., Peichl, M., Rambal, S., Raschi, A., Scott, R.L., Vaccari, F.P., van Gorsel, E., Varlagin, A., Wohlfahrt, G., Mahecha, M.D., 2018. Impacts of droughts and extreme-temperature events on gross primary production and ecosystem respiration: A systematic assessment across ecosystems and climate zones. Biogeosciences 15 (5), 1293–1318. http://dx.doi.org/10.5194/bg-15-1293-2018, URL: https://bg.copernicus.org/articles/15/1293/2018/.

Webb, E.K., Pearman, G.I., Leuning, R., 1980. Correction of flux measurements for density effects due to heat and water vapour transfer. Q. J. R. Meteorol. Soc. 106 (447), 85–100. http://dx.doi.org/10.1002/qj.49710644707, URL: https://rmets.onlinelibrary.wiley.com/doi/abs/10.1002/qj.49710644707.

Wilczak, J.M., Oncley, S.P., Stage, S.A., 2001. Sonic anemometer tilt correction algorithms. Bound.-Lay. Meteorol. 99 (1), 127–150. http://dx.doi.org/10.1023/A:1018966204465.

Wolf, S., Eugster, W., Ammann, C., Hani, M., Zielis, S., Hiller, R., Stieger, J., Imer, D., Merbold, L., Buchmann, N., 2014. Corrigendum: Contrasting response of grassland versus forest carbon and water fluxes to spring drought in Switzerland (2013 environ. Res. Lett. 8 035007). Environ. Res. Lett. 9 (8), 089501. http://dx.doi.org/10.1088/1748-9326/9/8/089501.

Wutzler, T., Lucas-Moffat, A., Migliavacca, M., Knauer, J., Sickel, K., Šigut, L., Menzer, O., Reichstein, M., 2018. Basic and extensible post-processing of eddy covariance flux data with REddyProc. Biogeosciences 15 (16), 5015–5030. http://dx.doi.org/10.5194/bg-15-5015-2018, URL: https://www.biogeosciences.net/15/5015/2018/.

Zhang, Y., Xiao, X., Zhou, S., Ciais, P., McCarthy, H., Luo, Y., 2016. Canopy and physiological controls of GPP during drought and heat wave. Geophys. Res. Lett. 43 (7), 3325–3333. http://dx.doi.org/10.1002/2016GL068501, URL: https://agupubs.onlinelibrary.wiley.com/doi/abs/10.1002/2016GL068501.